Hindawi
International Transactions on Electrical Energy Systems
Volume 2023, Article ID 6038394, 14 pages
https://doi.org/10.1155/2023/6038394

Research Article

Single-Phase Wireless Electric Vehicle Charger Using EF_2 Inverter

Soumya Ranjan Meher and Rajeev Kumar Singh

Department of Electrical Engineering, Indian Institute of Technology (BHU), Varanasi, India

Correspondence should be addressed to Soumya Ranjan Meher; soumyarmeher.rs.eee17@iitbhu.ac.in

Received 3 January 2023; Revised 1 May 2023; Accepted 17 May 2023; Published 30 June 2023

Academic Editor: Mouloud Denai

This paper proposes a wireless battery charger topology for electric vehicle (EV) application that can be installed in public charging infrastructure as well as in home premises. The proposed topology can maintain constant current as well as constant voltage at the battery terminal and simultaneously can maintain near unity power factor at the input side using power factor correction (PFC) operation and thus satisfy all the criteria of a standard EV charger. The heart of the wireless power transfer (WPT) scheme is a high-frequency (HF) inverter. In this work, a class EF_2 inverter is used to generate HF AC in such a way that it can deliver power with variable loading condition while maintaining constant current (CC) or constant voltage (CV) according to the requirement of CC-CV charging profile. To supply power to this EF_2 inverter, an AC-DC front-end converter (stage-1) is integrated with the charger. The stage-1 is operated as a constant voltage source to the EF_2 inverter for CC mode and constant current source for CV mode operation. CC-CV at the battery end and PFC at the input end are achieved only by controlling the gate pulse of stage-1. The WPT coils are first simulated using Ansys Maxwell package, and the complete charger is simulated with PSIM simulation software. A scaled-down 200 W laboratory prototype of the proposed charger is developed and tested with a resistive load to validate the idea. The wireless power transfer is achieved for a maximum distance of 12 cm between the transmitting and receiving coil. Finally, the charger is tested to charge both 12 V and 24 V battery packs and the CC-CV charging profile is presented for the 24 V, 30 Ah battery pack.

1. Introduction

Wireless charging for electric vehicle (EV) is one of the spellbinding research topics for power electronics engineers in recent times. The lack of public charging infrastructure in many countries leads the government to mandate manufacturers to include the charging circuit with the vehicle. This charging circuit is known as an on-board charger that is capable of charging the battery pack by tapping power from the utility grid without any additional infrastructure [1–3]. The on-board charger generally uses a wired connection, which is often messy, and this adds to the total weight of the vehicle, which is undesirable [4, 5]. The wireless EV charging system reduces the weight burden on the vehicle because it only contains a receiving coil and a rectifier unit as most of the power electronics interfaces are ousted from the vehicle to the transmitting side. A pictorial representation of a typical single-phase domestic/commercial wireless EV charging system is represented in Figure 1. Thus, wireless EV charging offers contactless power transfer and lighter on-board charging system [6–8]. An overview of wireless power transfer technology for EV charging is presented in [9].

The basic concept of wireless power transfer (WPT) lies in transmitting a high-frequency sinusoidal AC wave from the transmitting side to the receiving side without any wired connection [10, 11]. Instead of using a conventional step-up cycloconverter for producing high-frequency AC (HFAC) from the grid supply, an inverter is preferred to generate HFAC by operating this inverter at high switching frequency. So, a high-frequency inverter (HF inverter) is considered as the heart of the WPT system, which requires a DC source at its input to produce HFAC. Conventional WPT system uses an H-bridge inverter with filtering elements, operated at high frequency to generate HFAC [12–16]. Higher number of switches and hard switching of MOSFETs in case of H-bridge inverter are the two major

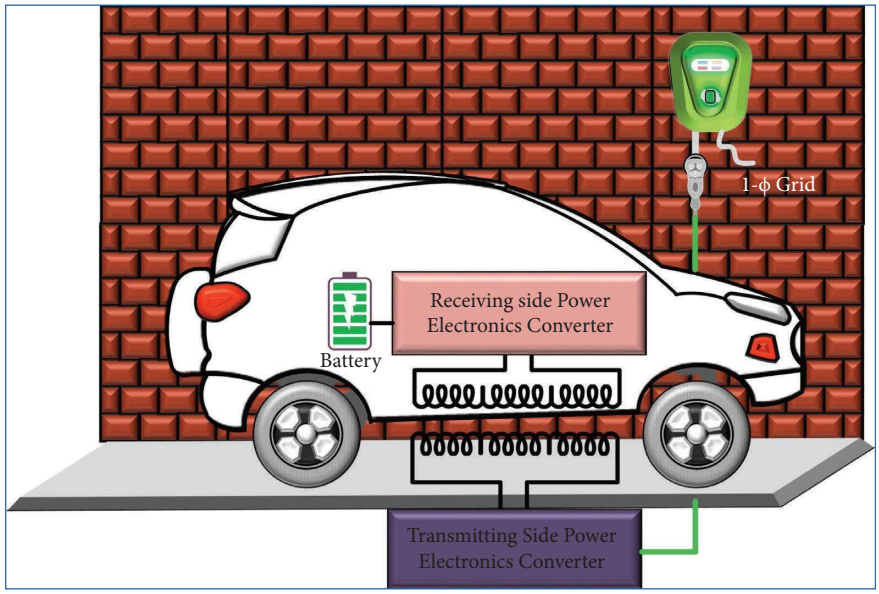

Figure 1: A pictorial representation of a typical wireless EV charging facility.

concerns, which led to the introduction of resonant inverters for WPT applications.

Many resonant inverters using resonance network with H-bridge inverter are discussed in [17]. Moreover, resonant inverters with minimum switches such as class D and class E inverters are reported in the literature [18–20], which are mostly preferred due to their soft switching property. Class E inverters are widely used in WPT application as these use only a single switch to produce HFAC which is also capable to achieve zero voltage switching (ZVS) for reducing the switching losses, which is well documented in [20]. Major concern in case of a class E inverter is the higher voltage stress during the off period across the switch caused by the resonating elements that are responsible for producing sinusoidal current at the output. This extra voltage stress on the switch reduces the power processing capability of the inverter. To overcome this, class EF_2 inverter is reported in [21], where an additional series L-C series network is used in parallel with the switch to reduce the voltage stress. The class EF_2 inverter is capable to achieve zero voltage switching (ZVS) as well as zero derivative switching (ZDS). But this topology is only applicable for a constant load resistance at the output. When the load resistance is changed to a value other than the designed value, the soft switching operation (e.g., ZVS and ZDS) is lost.

During the charging process of a battery, as the internal resistances of the battery continuously increase with the increase in the state of charge (SoC), the inverter used in the wireless charger should be capable to handle variable load resistance. To accommodate variable load resistance, a class EF_2 inverter with load independent criteria is discussed in [22]. The reported class EF_2 inverter behaves as a constant AC current source for variable load resistance at the output. However, to verify the load independent criteria, researchers have used a fixed load resistance of 50 Ω at the secondary side of the WPT and the distance between the transmitting coil and receiving coil was varied to demonstrate the variable load resistance reflected across the output of EF_2 inverter as an outcome of change in distance.

To implement the CC-CV charging technique, the charger should behave as a source of constant current during CC mode and a source of constant voltage during CV mode. The earlier reported class EF_2 inverter can be implemented for CC mode, but it fails to deliver power to the battery during CV mode. Additionally, the EF_2 inverter uses a DC source as its input to provide AC power at high frequency. Drawing power from the AC grid is more convenient as the grid is more reliable and easily available everywhere as compared to any DC power source.

In order to address all these issues, this paper proposes a wireless EV charger that taps power from the single-phase AC supply and charges the EV battery pack wirelessly satisfying both constant current and constant voltage operation. The transmitting side power converters with the transmitting coil are placed beneath the ground level, and the receiving coil with rectifier unit is fitted with the vehicle. The idea is to charge the EV battery pack mostly during night time, when the vehicle is parked in home garage.

Overall contribution of this paper is listed as follows:

(i) The proposed charger is designed to be implemented at any charging station specifically for home garage as it draws power from single-phase grid.

(ii) The EF_2 inverter used in the proposed charger is capable to deliver power in both CC and CV modes throughout the designed range of load variation.

(iii) Switching scheme with fixed duty ratio is implemented for EF_2 inverter to avoid fast sensing requirement of variable AC voltage and current that also needs high-speed controller response as the inverter is operated at very high frequency.

(iv) The proposed charger ensures CC-CV charging of the battery as well as power factor correction (PFC) operation at the input side with only one controlled signal.

1.1. Paper Organization. Section 2 of this paper describes the system configuration with complete circuit diagram. Design and operation of the complete charger are described in Section 3. Necessary mathematical modelling and analysis are also included in this section. Section 4 describes the control strategy of the charger with proper schematics. The proposed charger is verified experimentally as well as using simulation platforms, which are discussed in Section 5. The paper is finally concluded in Section 6.

2. Proposed Wireless EV Charger

The proposed charger taps power from the single-phase utility supply and wirelessly charges the battery set of EV. The circuit diagram of the proposed topology is shown in Figure 2. The proposed circuit is divided into four major subsections: (i) AC-DC boost converter, (ii) DC-HFAC resonant inverter, (iii) wireless power transfer scheme, and (iv) rectifier unit.

As discussed earlier, a HF inverter is the heart of WPT scheme. A load independent EF_2 inverter is used to produce high-frequency sinusoidal AC. The HF inverter produces constant AC current when excited with constant DC voltage and produces constant AC voltage when the input of the inverter is a constant DC current source. To accommodate either a constant DC voltage source or a constant DC current source at the input of the inverter, an AC-DC front-end converter is selected as stage-1. The front-end converter is responsible to deliver power to the EF_2 inverter at constant voltage or constant current while maintaining the input power factor to near unity. The WPT scheme uses the magnetic resonance coupling (MRC) technique to transfer power from the transmitting side to receiving side wirelessly. This consists of two coils (namely, primary and secondary) with their corresponding matching network. The primary coil draws power from the inverter and transmits to the secondary coil. The HFAC received at the secondary coil is converted to DC by a full-bridge diode rectifier that charges the battery.

3. Operation and Design

3.1. Stage 1: AC-DC Boost Converter. A bridge-less PFC structure with two switches on the lower side, two diodes on the upper side, and an inductor at the input is used as an AC-DC boost converter. This stage is responsible to deliver DC power to the HF inverter and to maintain near unity power factor at the grid side. The inductor at the input side acts as a boost inductor for this stage. The operation of this stage is described with four modes of operations as shown in Figure 3.

During positive half cycle of input AC supply, diode D_A, switch S_A, and body diode of switch S_B (D_{SB}) are forward biased. When the switch S_A is turned ON, current gets a shortest path through S_A and flows through the input inductor, node A, switch S_A, body diode D_{SB}, and node B as shown in Figure 3(a). The boost inductor is charged during this mode. When the switch S_A is turned OFF, current will flow through inductor, node A, diode D_A, load, body diode D_{SB}, and node B as shown in Figure 3(b) ensuring the smooth discharge of energy stored in the inductor L_{in} during previous mode. Though, due to the positive nature of supply voltage, diode D_1 should be forward biased, turning ON of switch S_A makes this reverse biased during mode 1, but it is forward biased during mode 2.

Similarly, for negative half cycle, while the switch S_B is ON, the inductor is charged with the current, flowing through node B, switch S_B, body diode D_{SA}, and node A as shown in Figure 3(c). In mode 4, the stored energy in the inductor will be discharged to the load as shown in Figure 3(d).

In both the positive and negative half cycles of input supply, the charging of input inductor during the switch ON period and discharging of inductor during the switch OFF period confirm the boost operation.

3.2. Stage 2: High-Frequency EF_2 Inverter. The proposed schematic uses an EF_2 inverter to produce high-frequency AC voltage or current according to the requirement of CC-CV charging algorithm. Figure 4 shows the circuit representation of the class EF_2 inverter that supports both CC and CV modes of operation by delivering constant AC current and constant AC voltage during CC mode and CV mode, respectively, which is analyzed in this subsection. The equivalent circuit diagrams during ON state and OFF state of the switch S_{inv} are presented in Figures 5(a) and 5(b), respectively.

While the inverter is excited with a constant DC voltage source, assuming a sinusoidal output current of the inverter,

$$I_{out} = I_m \sin(\omega t + \phi). \tag{1}$$

During ON state of the switch S_{inv} (Figure 5(a)) (for $0 \le \omega t < 2\pi D$), voltage across the switching MOSFET can be written as

$$V_{DS}(\omega t) = 0. \tag{2}$$

Current through the capacitor C_1 is $i_{C1} = 0$.

As the voltage across the switch is zero, it is rewritten as

$$v_{L2} + v_{C2} = 0 \Longrightarrow L_2 \frac{d(i_{L2})}{dt} + \frac{1}{C_2} \int i_{L2} \mathrm{d}t = 0. \tag{3}$$

Differentiating the above equation and solving the second-order differential equation, solution for i_{L2} is obtained. Again, normalizing i_{L2} with respect to I_{IN} will be in the form of

$$\frac{i_{L2}}{I_{IN}} = A_1 \cos(q_1 \omega t) + B_1 \sin(q_1 \omega t). \tag{4}$$

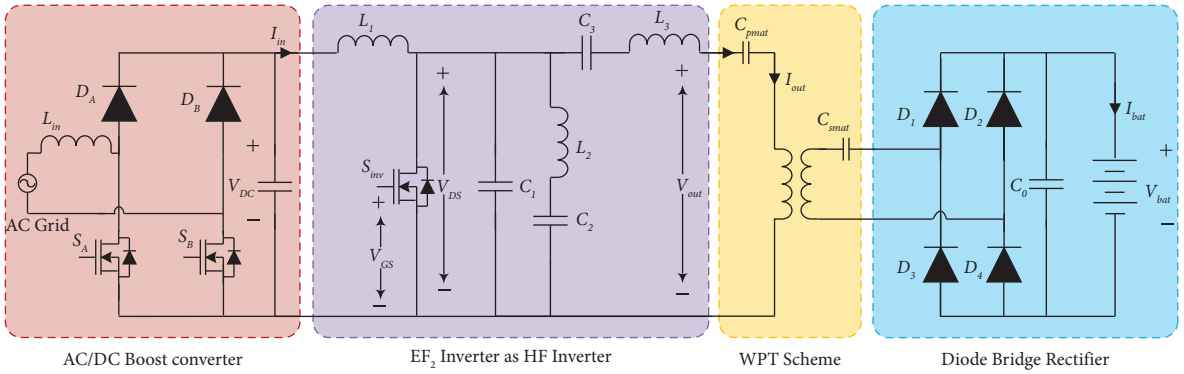

Figure 2: Complete circuit schematics of the proposed wireless EV charger.

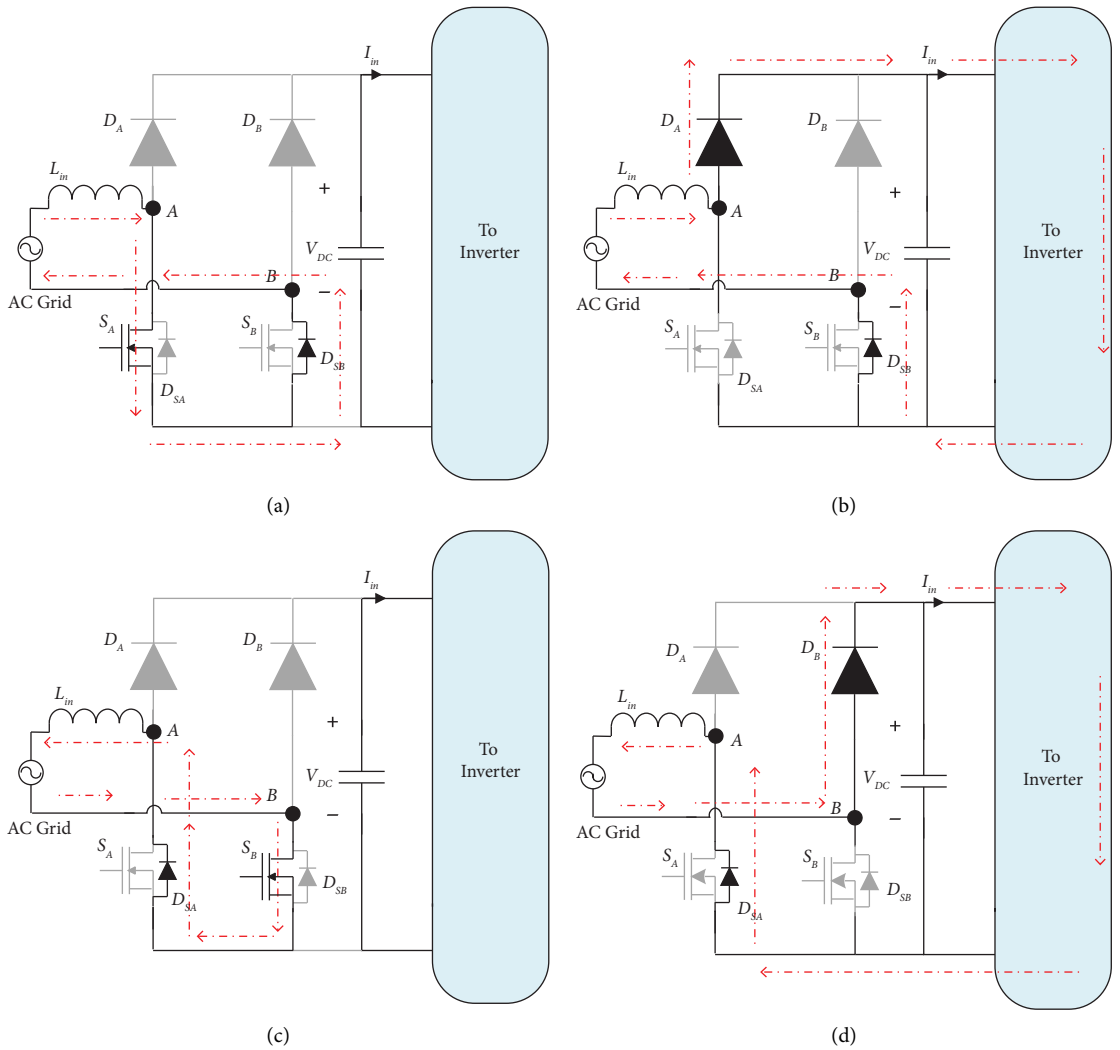

Figure 3: Operation of front-end converter in different modes.

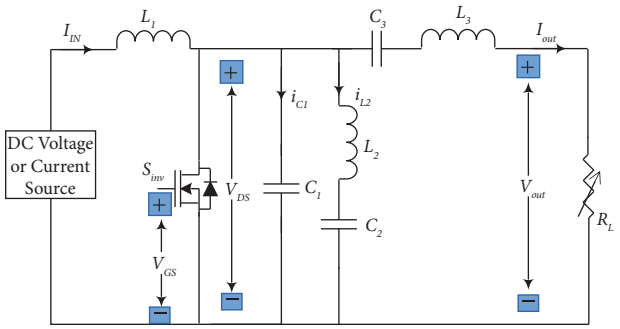

Figure 4: Circuit diagram of EF_2 inverter.

During OFF state of the switch (Figure 5(b)) $(2\pi D \le \omega t < 2\pi)$,

$$i_{DS} = 0, \tag{5}$$

$$i_{L2} = I_{IN} - I_m \sin(\omega t + \phi) - \omega C_1 \frac{d}{d\omega t} V_{DS}(\omega t). \tag{6}$$

Use

$$V_{DS} = \omega L_2 \frac{di_{L2}(\omega t)}{d\omega t} + \frac{1}{\omega C_2} \int_{2\pi D}^{\omega t} i_{L2}(\omega t) d\omega t + v_{C2}(2\pi D). \tag{7}$$

As solved for the ON state, $V_{DS} = 0$.

Solving (7) for i_{L2} and normalizing the expression of i_{L2} with respect to I_{IN}, it can be written as

$$\frac{i_{L2}}{I_{IN}} = A_2 \cos(q_2 \omega t) + B_2 \sin(q_2 \omega t) - \frac{{q_2}^2 p}{{q_2}^2 - 1} \sin(\omega t + \phi) + \frac{1}{k+1}, \tag{8}$$

where

$$k = \frac{C_1}{C_2}, \tag{9}$$

$$q_2 = \frac{1}{\omega} \sqrt{\frac{C_1 + C_2}{L_2 C_1 C_2}} = q_1 \sqrt{\frac{k+1}{k}}, \tag{10}$$

$$p = \frac{C_2}{C_1 + C_2} \frac{I_m}{I_{IN}} = \frac{1}{k+1} \frac{I_m}{I_{IN}}, \tag{11}$$

where A_1, B_1, A_2, and B_2 are the arbitrary constants considered for solving the differential equations during both ON and OFF modes. These arbitrary constants are determined based on boundary conditions of inductor currents and capacitor voltages.

Using KCL at drain node,

$$i_{C1}(\omega t) = I_{IN} - I_m \sin(\omega t + \phi) - i_{L2}(\omega t). \tag{12}$$

Normalizing $i_{C1}(\omega t)$ with respect to I_{IN},

$$\frac{i_{C1}}{I_{IN}}(\omega t) = 1 - p(k+1)\sin(\omega t + \phi) - \frac{i_{L2}}{I_{IN}}(\omega t). \tag{13}$$

Using boundary conditions,

$$i_{L2}(2\pi D^-) = i_{L2}(2\pi D^+), \tag{14}$$

$$i_{L2}(0) = i_{L2}(2\pi), \tag{15}$$

$$\left.\frac{d(i_{L2})}{d\omega t}\right|_{2\pi D^-} = \left.\frac{d(i_{L2})}{d\omega t}\right|_{2\pi D^+}, \tag{16}$$

$$\left.\frac{d(i_{L2})}{d\omega t}\right|_{0} = \left.\frac{d(i_{L2})}{d\omega t}\right|_{2\pi}. \tag{17}$$

During switch OFF period, voltage across the switch is the same as voltage across the capacitorC_1:

$$V_{DS} = \frac{1}{\omega C_1} \int_{2\pi D}^{\omega t} i_{C1}(\omega t) d\omega t \Longrightarrow \frac{V_{DS}}{V_{IN}} = \frac{I_{IN}}{\omega C_1 V_{IN}} \beta(\omega t), \tag{18}$$

where

$$\beta(\omega t) = \int_{2\pi D}^{\omega t} \frac{i_{C1}(\omega t)}{I_{IN}} d\omega t. \tag{19}$$

V_{DS} can be written as follows using equations (13) and (19) and the ZVS conditions.

$$V_{DS}(\omega t = 2\pi) = 0 \Longrightarrow \beta(2\pi) = 0. \tag{20}$$

Using all the above conditions and considering maximum power output capability ($q_1 = 1.66$ and $k = 1.2706$) as discussed in [22], the expressions for the circuit parameters at 200 kHz are found and given in Table 1. The same expressions are also valid for constant voltage operation.

3.3. Stage 3: Wireless Power Transfer Scheme. The transmitting and receiving coils are designed according to the required current rating. Series-series topology is considered as the compensating network for MRC. A combination of capacitor in series with the coil at both transmitting and receiving sides forms the WPT section as shown in Figure 2. Values of these capacitors (C_{pmat} and C_{smat}) are designed to resonate with the corresponding coil inductances at the operating frequency using $f_s = (1/2\pi\sqrt{LC})$. Same number of turns are used in both transmitting and receiving side coils, which facilitate to use same values of capacitances in both sides, i.e., $C_{\text{pmat}} = C_{\text{smat}}$.

3.4. Stage 4: Rectifier Unit. The rectifier unit uses a simple full-bridge diode rectifier to convert the HFAC to DC as shown in Figure 2. The selection of diodes is of major concern, as the high-frequency operation requires less

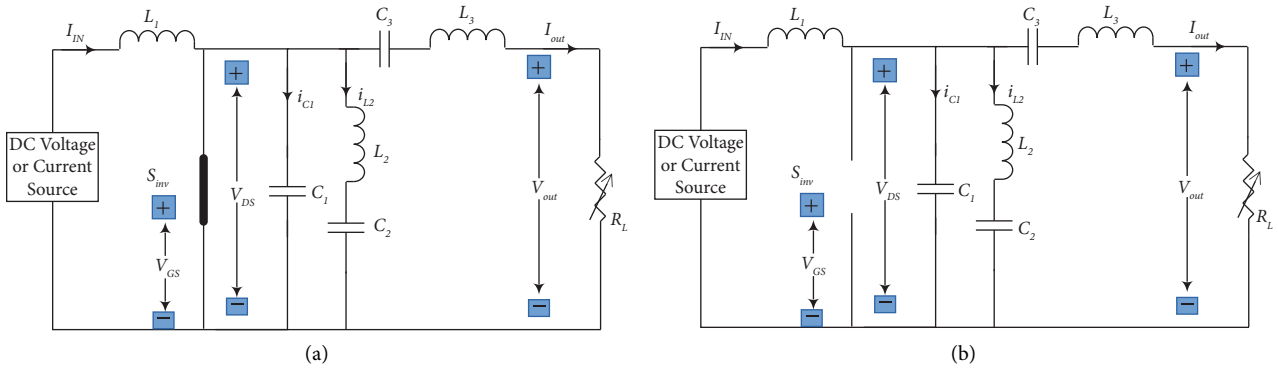

Figure 5: (a) Equivalent circuit diagram of inverter during ON period. (b) Equivalent circuit diagram of inverter during OFF period.

Table 1: Expressions for EF_2 circuit parameters.

Parameter	Expressions
C_1	$(1.41011/R_L \times 10^7)$
C_2	$(C_1/1.2706)$
L_x	$(2.1543/C_1 \times 10^{13})$
L_3	$(7.95 \times Q * R_L/10^7)$
C_3	$(6.3325/(L_3 - L_x) \times 10^{13})$
L_2	$(2.2980/C_2 \times 10^{13})$

reverse recovery time. The output capacitor of this unit is designed to minimize the ripple in output voltage.

4. Control Scheme for the Proposed Wireless EV Charger

The most important section of the proposed transmitting side topology is the EF_2 inverter. Closed-loop operation of such high-frequency inverter is difficult, as this requires the sensing of HF inverter output parameters. The sensing of high-frequency parameter requires even higher frequency of controller operation. To avoid these issues, the EF_2 inverter is operated with constant duty ratio and constant switching frequency.

This HF inverter requires a regulated voltage or current source at its input for CC-CV operation. To achieve this, the front-end converter (stage-1) needs to be operated accordingly. For the front-end converter to supply regulated voltage/current at its output terminal, its output voltage and current need to be sensed. But as the EF_2 inverter is operated at constant duty cycle, the required voltage and current at the battery terminal can be multiplied by a gain factor to find the new reference values of voltage or current at the output of stage-1. Therefore, instead of sensing voltage and current at the output of stage-1, these can be sensed at the battery terminal and corresponding gain factor can be multiplied. These signals are then compared with their corresponding reference signals, and using proper controllers, the PWM signals are generated for the front-end converter. The PWM pulses are used to switch the MOSFETs S_A and S_B in order to achieve regulated voltage or current at the output of the front-end converter as well as the PFC operation at the input grid side.

4.1. CC Mode. In CC mode, a constant amount of current is dumped into the battery. When the HF inverter is operated with a suitable fixed duty ratio and the input excitation is a constant DC voltage source, it will deliver sinusoidal AC current with constant magnitude throughout the range of load variation, for which it is designed. The battery terminal current is sensed and compared with its reference value and corresponding PWM signal is generated to maintain constant voltage at the input of HF inverter. The corresponding control scheme is shown in Figure 6(a).

4.2. CV Mode. During CV mode, the battery is charged with a constant terminal voltage, where the charging current decreases gradually with the increase in state of charge (SoC) of the battery. To support this, the charger should deliver power while maintaining the output voltage constant. For maintaining constant voltage at the battery terminal, the HF inverter should be capable to provide constant voltage at its output. As discussed earlier, the front-end converter is operated to act as a source of constant DC current for the inverter.

In this mode, the battery terminal voltage (V_{bat}) is compared with its reference value (V_{ref}) and fed to the PI controller. In a similar way to CC mode, the PI controller generates the required PWM signal in order to make the front-end converter as a source of constant current to feed the HF inverter as shown in Figure 6(b).

During both the modes, the HF inverter operates at a constant duty ratio. CC-CV logic is implemented to decide the mode of operation according to the SoC of the battery. During low SoC, the battery is charged with constant current, and at high SoC, the battery is charged with a constant voltage. The transition from CC mode to CV mode is decided based on the battery terminal voltage. The charger remains in CC mode until the battery voltage reaches the full voltage as mentioned in the manufacturer's data sheet. Once the battery voltage reaches the full voltage level, then the controller forces the charger to enter into CV mode of operation. Accordingly, the front-end converter is operated to behave as a regulated source of current or voltage. A single PI is sufficient to deliver power to the inverter at regulated voltage or current during both CC and CV modes.

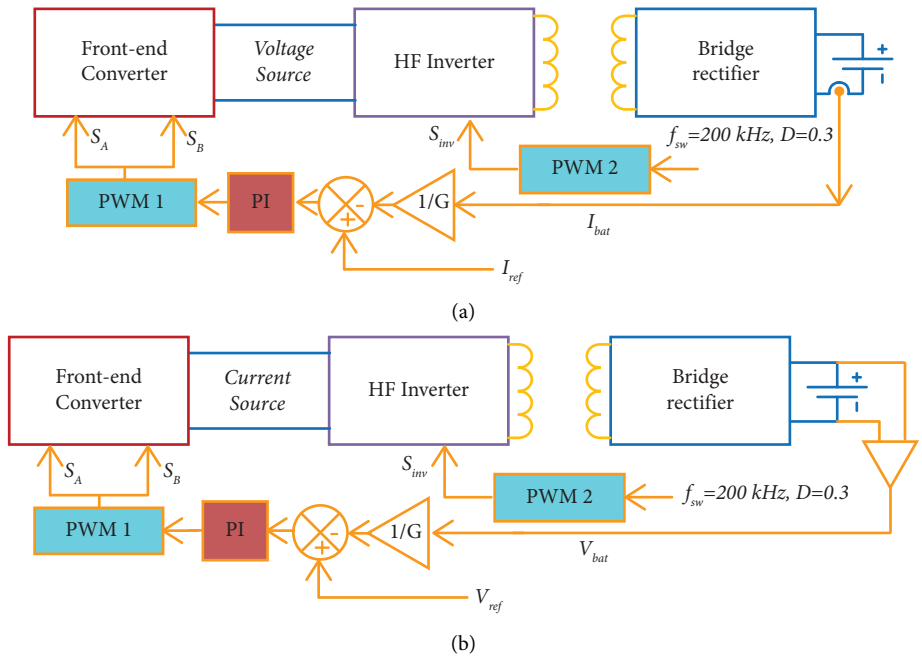

Figure 6: (a) Control scheme for CC mode of operation. (b) Control scheme for CV mode of operation.

It is necessary to maintain near unity power factor at the input side as the proposed wireless charger taps power from the single-phase supply for charging the EV battery pack. To implement PFC operation at the grid side, input AC voltage and current are sensed and fed to the PFC controller. The combined effort of PI and PFC controller is then fed to the PWM block. The final PWM signals are fed to the gate driver circuits of two lower switches of the front-end converter. The complete control scheme for the proposed wireless charger is implemented using a TMS320F28335 DSP experimenters' kit from Texas Instruments and is shown in Figure 7. The reference values in the CC-CV logic are decided based on the required charging current and charging voltage of the battery.

5. Experimental Verification

The primary and secondary coils of the WPT system are simulated for demonstrating the strength of magnetic field intensity (B) in and around the coils and are presented in Figure 8. The color coding of its strength in Tesla is also shown in Figure 8. Considering the leakage and mutual inductances from Ansys, the complete topology is simulated using PSIM to verify the constant current and constant voltage property of the proposed charger. The aim is to test the charger with dynamic load condition as the battery is a dynamic load during its charging operation. Therefore, the charger is tested with resistive load and the load resistance across the DC terminal is changed instantaneously to check the robustness of the charger. The dynamics are captured for both constant current and constant voltage mode using simulation platform. The corresponding results for CC and CV modes are given in Figures 9(a) and 9(b), respectively.

A scaled-down laboratory prototype of the proposed wireless charger is developed and verified to charge a 24 V, 30 Ah battery set as shown in Figure 10. The proposed wireless EV charger is also verified in the laboratory with a resistive load to wirelessly transfer 191 W of power with a distance of 120 mm between the primary and secondary coils. The required air gap between the transmitting coil and the receiving coil depends on the minimum ground clearance required by a vehicle as the transmitting (primary) coil is usually kept at the ground level and the receiving (secondary) coil is fitted just below the vehicle. Ground clearance for a light motor vehicle (LMV) is normally in the range of 120 mm to 150 mm. In order to test the effectiveness of wireless power transfer (WPT) system, the proposed charger is tested with a distance of 120 mm between the primary and secondary coils.

A 4.5 mH inductor is used at the input AC side to boost the input voltage as well as to smoothen the ripple of input AC current. A Semikron IGBT module is used to realize the AC-DC boost stage. Circuit parameters of EF_2 inverter are derived for a switching frequency of 200 kHz, and the corresponding values are given in Table 2. The WPT coils are designed according to the Ansys design and connected at the output terminals of EF_2 inverter as shown in Figure 10. Figure 11 shows the clear view of the PCB implementing EF_2 inverter using a GaN MOSFET. Si or SiC MOSFET can also be used to implement a switching frequency of 200 kHz, but reason behind considering GaN MOSFET in this work is to increase the switching frequency in the order of MHz. The WPT section with transmitting and receiving side coil is shown in Figure 12.

A four-layer FR4 PCB board is designed to implement the EF_2 inverter as shown in Figure 11. Special care is taken while fabricating the SMD components especially GaN

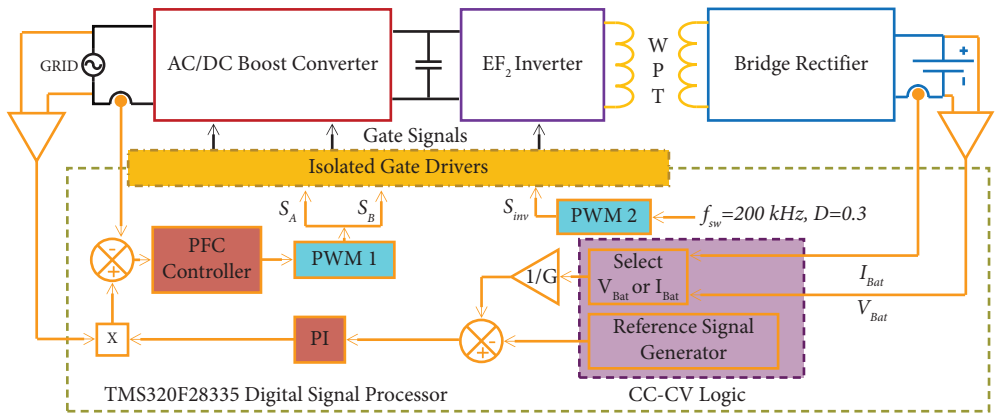

Figure 7: Control schematic for the proposed wireless EV charger.

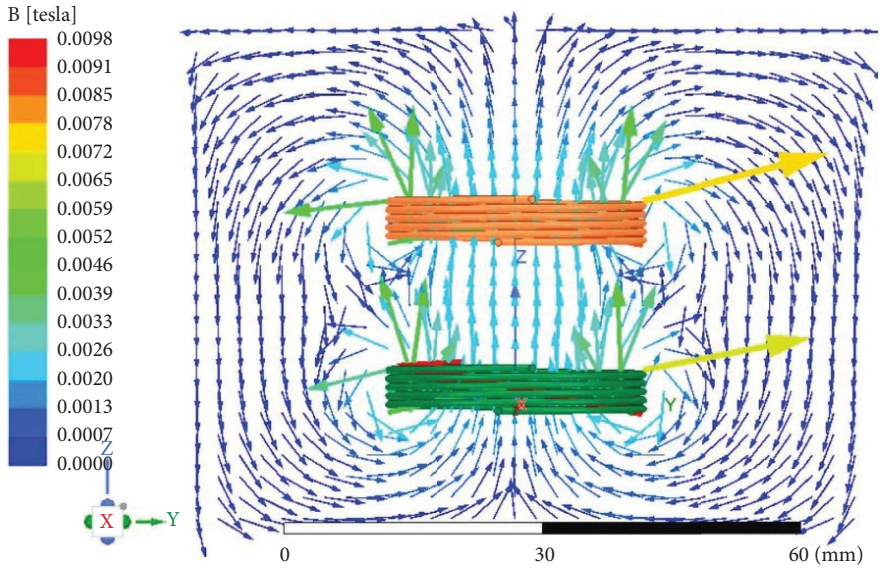

Figure 8: Coil structure designed using Ansys Maxwell package with its analysis on magnetic field intensity.

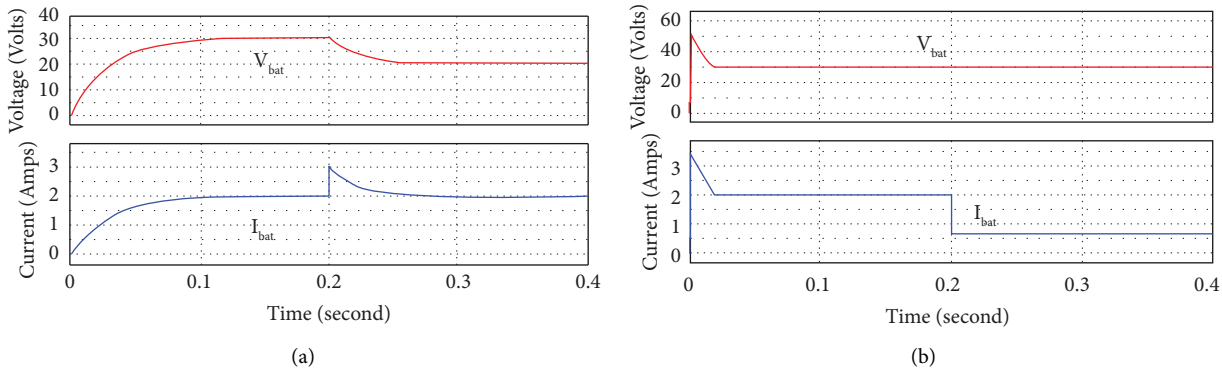

Figure 9: Simulation results of the proposed charger validating (a) CC mode and (b) CV mode.

MOSFET. The GaN device is assembled on the board by properly following the reflow soldering process. An enhancement-mode high-electron mobility transistor (E-HEMT) GS66508B is used as S_{inv} for the HFAC inverter, which is a bottom-side cooled device. The recommended gate voltage range is 0 V to +6 V for optimal performance. Si-8271-GB-IS with proper biasing is used as a gate driver circuit for operating the GaN MOSFET. The bulky ferrite core-based inductors are replaced by lightweight air-core inductors to avoid saturation at high-frequency operation

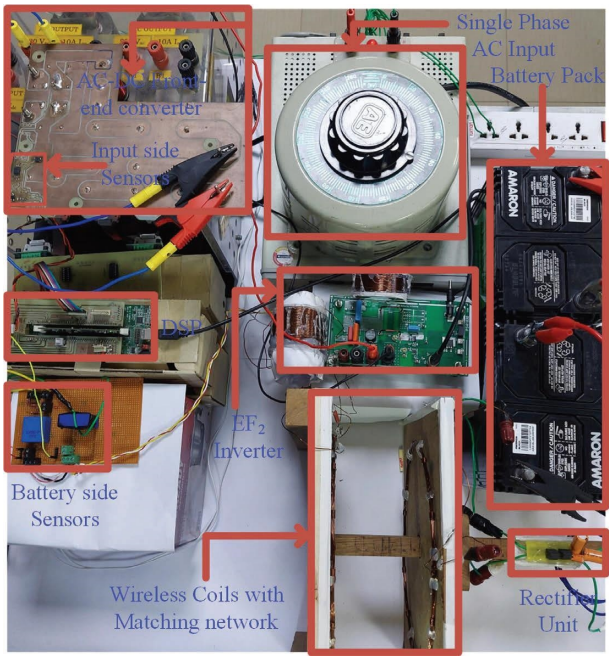

Figure 10: Experimental setup to verify the proposed idea.

Table 2: Circuit parameters.

Parameter	Rating
L_1	680 μH, 1200 mA
C_1	6800 pF, 1 kV
L_2	42 μH
C_2	5600 pF, 500 V
L_3	160 μH
C_3	5030 pF

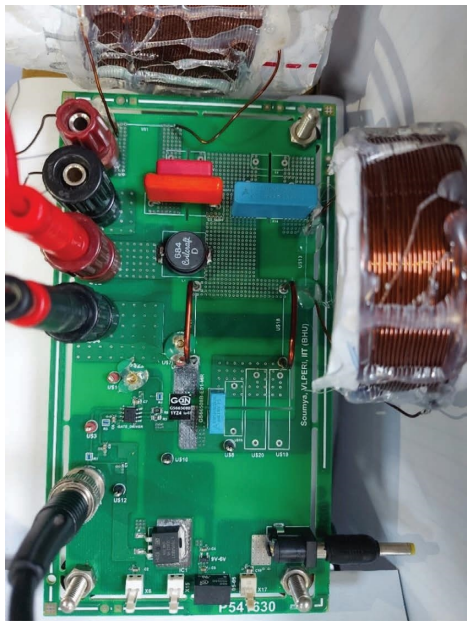

Figure 11: Four-layer PCB for implementing EF_2 inverter using GaN device.

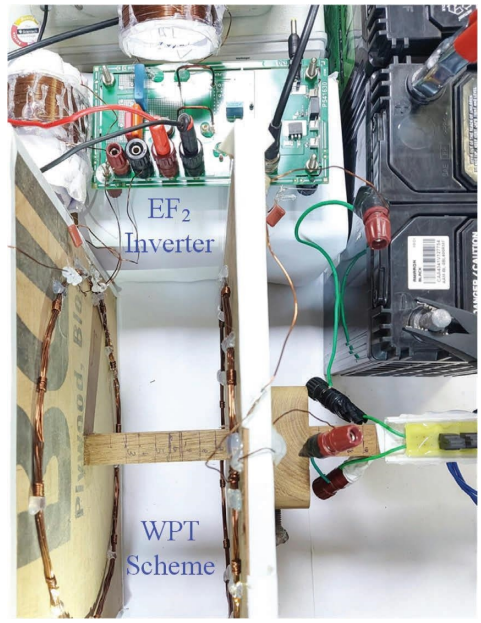

Figure 12: The WPT section showing the transmitting and receiving side coil.

except for L_1 as this is only responsible to reduce the current ripple at DC side of the inverter. A 684 uH SMD inductor is used for this purpose. These air-core inductors are designed using enamel painted single-strand copper wire of diameter of 0.85 mm. Metalized polypropylene capacitors are used to support high-frequency operation. The rating of inductors and capacitors used is shown in Table 2.

5.1. Operation of EF_2 Inverter. The EF_2 inverter is operated at a switching frequency of 200 kHz, and the results are shown in Figure 13. V_{GS} shows the gate pulse to the GaN, and V_{DS} shows the drain to source voltage of MOSFET, while I_{OUT} shows the output current supplied by the inverter. The output current is sinusoidal, and the frequency is same as the switching frequency. The voltage across the switch V_{DS} proves the ZVS operation of the inverter.

5.2. Proposed Charger with Resistive Load. The charger is verified with resistive load to ensure smooth operation for all probable conditions before charging the battery. Steady-state operation showing output voltage and current (V_0 and I_0) for a 20 Ω load while maintaining ZVS is shown in Figure 14. The transmitting side HFAC voltage and current along with voltage and current at the output terminal are shown in Figure 15. Use of proper matching networks at both the transmitting and receiving sides results in perfect sinusoidal voltage and current at the transmitter side. The charger is tested at nearly 200 W to transfer power wirelessly to a 20 Ω load. The corresponding result is shown in Figure 16, where the ZVS condition is achieved with 61 V output voltage and 3.12 A of output current. Figures 13, 14, and 16 show the peak and valley in V_{DS} waveform. This is due to the presence of the additional parallel network (L_2 in series with C_2) across the switch. This series combination across the switch

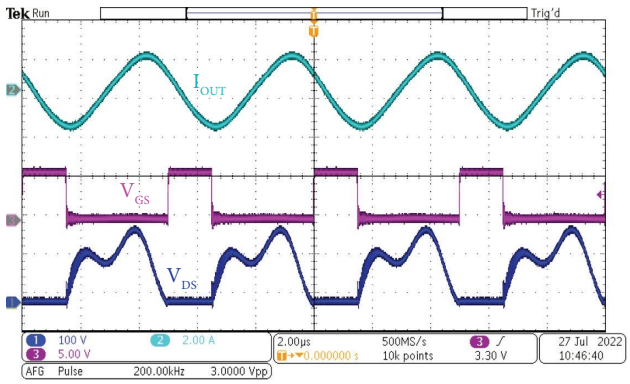

Figure 13: Operation of EF_2 inverter with high-frequency AC output current satisfying ZVS condition.

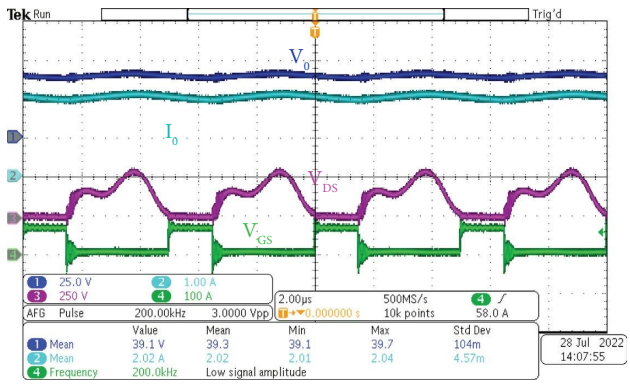

Figure 14: Steady-state operation of the proposed wireless charger with resistive load.

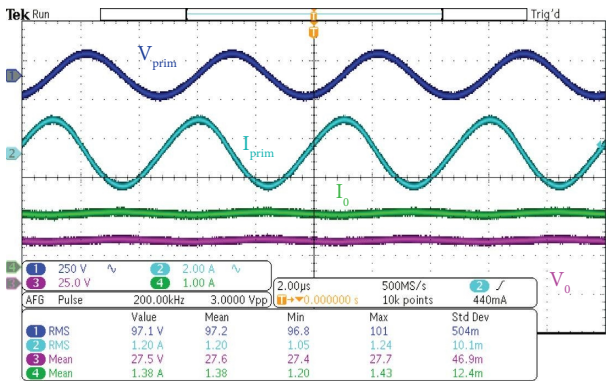

Figure 15: Steady-state operation of the proposed wireless charger with resistive load showing primary side voltage and current with output terminal voltage and current.

reduces the peak of V_{DS} as compared to class E inverter. The complete operation of class EF_2 inverter with relevant mathematical analysis is well documented in the literature [21, 22].

5.3. Charging a 12 V Lead-Acid Battery. A 12 V, 30 Ah lead-acid battery is charged to verify the validity of the proposed wireless charger. The CC-CV logic is designed to dump

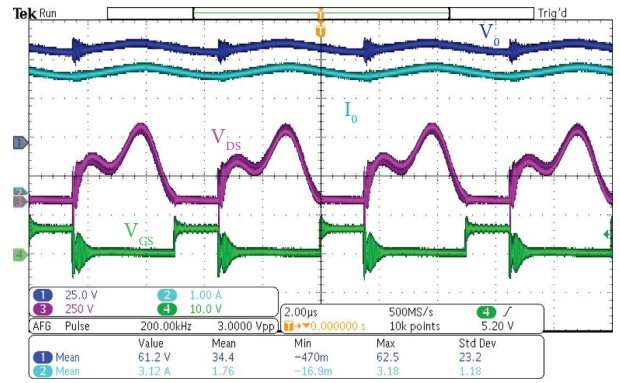

Figure 16: Steady-state operation of the proposed wireless charger supplying 191 W wirelessly to a resistive load.

a constant current of 1.11 A in CC mode and maintain a constant voltage of 14.5 V during CV mode. Figure 17 shows the CC mode, and Figure 18 shows the CV mode, where the charging current is decreasing gradually maintaining a constant voltage of 14.5 V.

5.4. Charging a 24 V Lead-Acid Battery. Finally, the proposed wireless charger is validated to charge a 24 V, 30 Ah battery set to obtain the CC-CV profile. Waveforms at different nodes are captured and discussed in this subsection. Figure 19 shows that the battery is charged in CC mode with a current of 1 A, and the result is captured when the battery terminal voltage reached 26.3 V. The transmitting side voltage and current during this period are also found to be sinusoidal, and the frequency is same as the switching frequency. The proposed charger draws power from the grid utility while maintaining near unity power factor at the grid side as shown in Figure 20(a). The zoomed-in result of Figure 20(a) is shown in Figure 20(b) to verify the sinusoidal nature of current delivered by the HF inverter as well as its smooth ZVS operation. Figures 21(a) and 21(b) show the PFC operation at the input side of the proposed charger and the sinusoidal voltage and current at the transmitting side of the WPT system.

Figure 22 shows both the transmitting and receiving side voltage and current during charging of the 24 V, 30 Ah battery set. This confirms the perfect wireless power transfer and correct matching network parameters associated with this. The battery terminal voltage and current with primary side current of EF_2 inverter satisfying ZVS operation are shown in Figure 23.

The grid side input to the charger and its battery terminal output while charging the 24 V, 30 Ah battery are shown in Figure 24. This shows that a constant amount of current is dumped into the battery during low SoC while maintaining near unity power factor at the input side. The CC-CV profile while charging the 24 V battery set is drawn and is shown in Figure 25, which confirms the implementation of CC-CV charging technique. The efficiency is measured during charging of both 12 V and 24 V batteries at different terminal voltages. The efficiency curves are prepared separately for both the batteries and are presented in Figure 26.

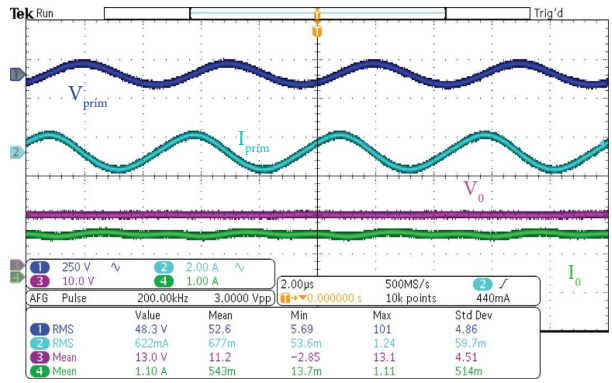

Figure 17: Primary side parameters with terminal voltage and current while charging the 12 V battery in CC mode.

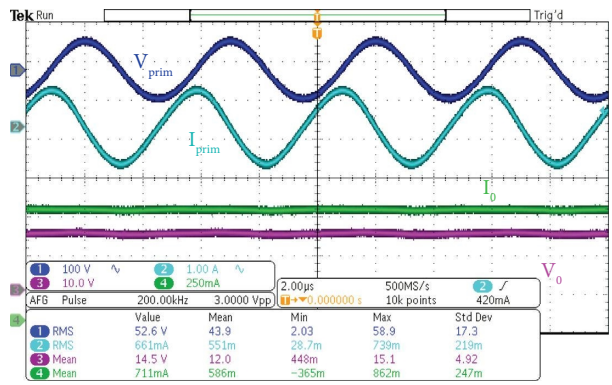

Figure 18: Primary side parameters with terminal voltage and current while charging the 12 V battery in CV mode.

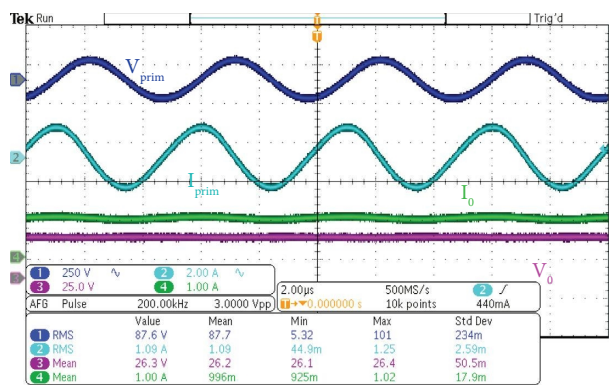

Figure 19: Primary side parameters with terminal voltage and current while charging the 24 V battery.

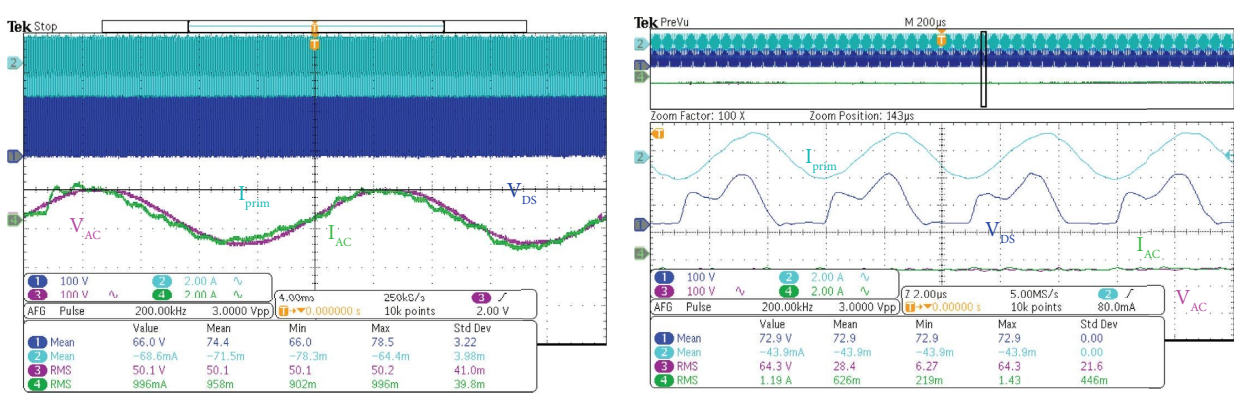

(a) (b)

Figure 20: Operation of the proposed charger with 24 V battery. (a) PFC at grid side. (b) ZVS of the EF_2 inverter in zoomed view.

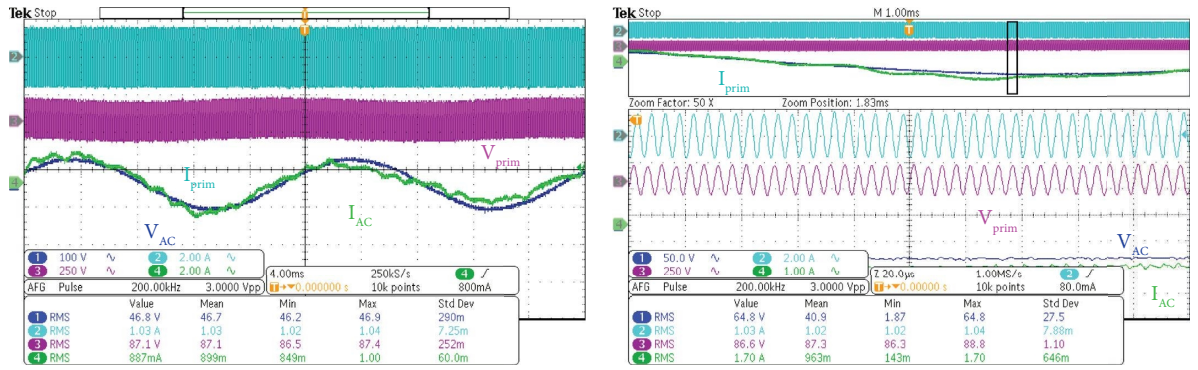

(a) (b)

Figure 21: Operation of the proposed charger while charging a 24 V battery. (a) Demonstrating PFC operation at the grid side. (b) Zoomed view of the voltage and current at the transmitting side.

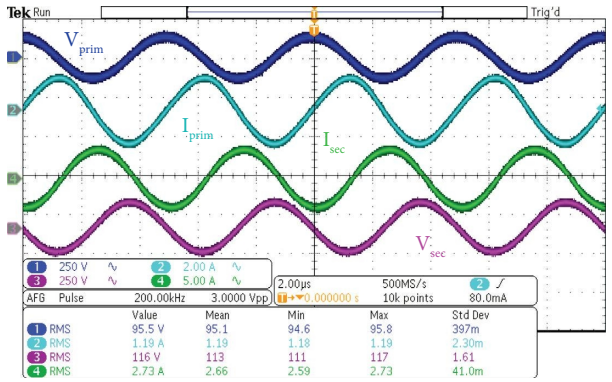

Figure 22: Operation of wireless power transfer scheme showing transmitting and receiving side voltages and currents while charging the 24 V battery.

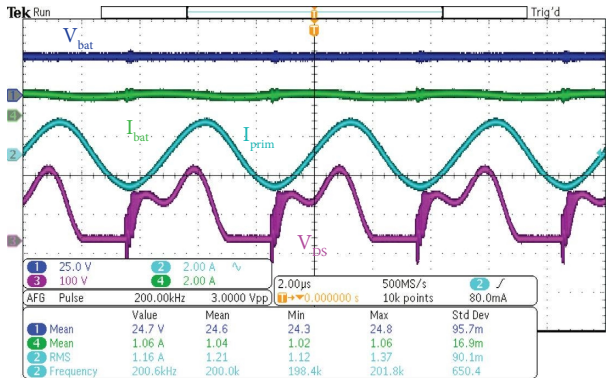

Figure 23: Battery terminal voltage and current demonstrating ZVS operation with sinusoidal output current of EF_2 inverter.

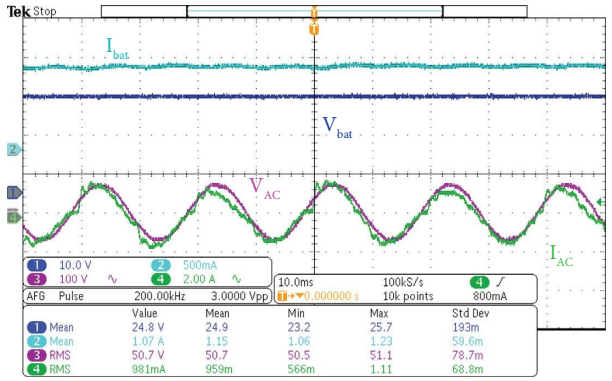

Figure 24: Battery terminal parameters with input side voltage and current maintaining near UPF at the grid side.

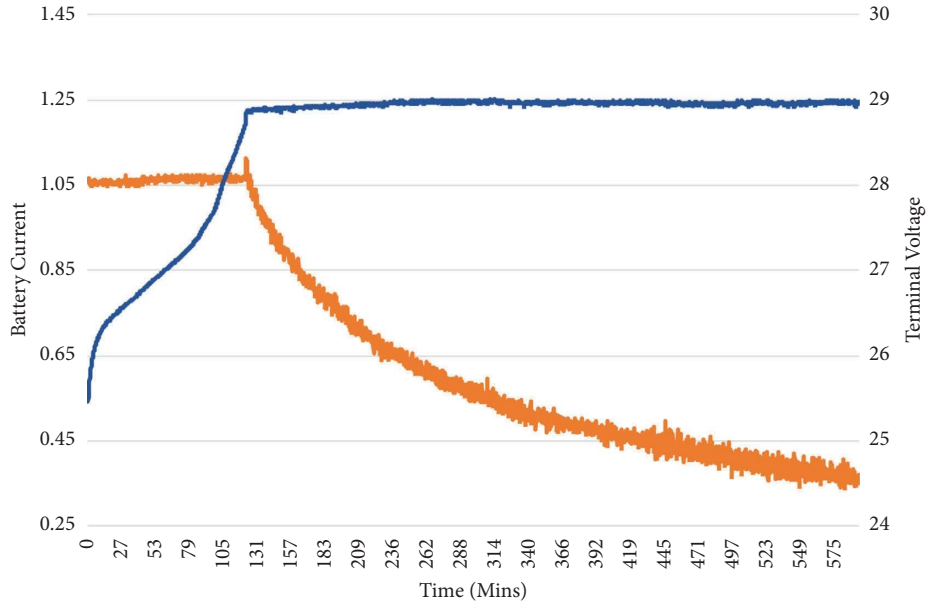

Figure 25: CC-CV charging profile of the 24 V, 30 Ah battery.

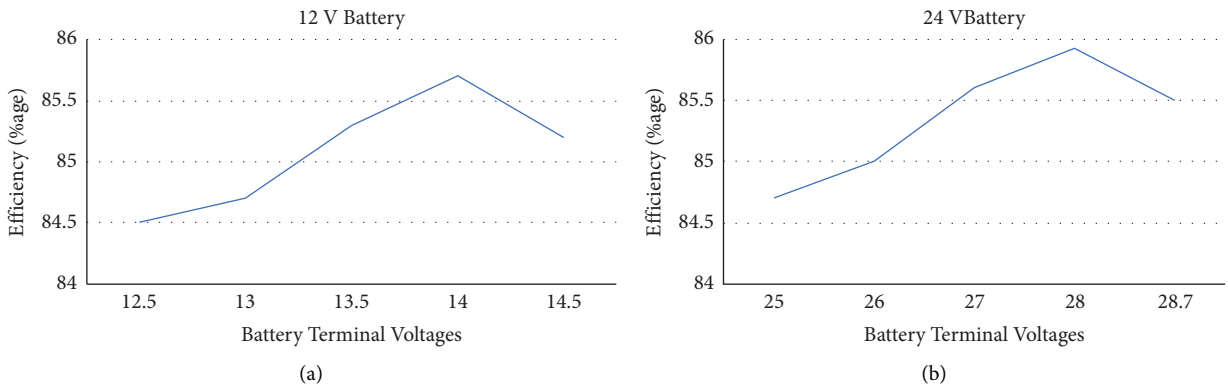

Figure 26: Efficiency curve during charging of (a) 12 V battery and (b) 24 V battery.

6. Conclusion

A wireless battery charger for electric vehicle (EV) applications is proposed in this paper. The proposed topology is capable to charge the EV battery pack wirelessly by taking power from a single-phase wall outlet available in domestic premises. The control scheme of the charger ensures power factor correction (PFC) operation at the input grid side along with CC-CV charging of the battery. During CC mode, the AC-DC stage supplies DC power at constant voltage to the EF_2 inverter, which produces constant AC current at high frequency. At the receiving side, this constant HFAC current is rectified to charge the battery with constant DC current. Similarly, during CV mode, the EF_2 inverter is fed by the AC-DC stage with constant current for producing constant HFAC voltage at the output of inverter. The constant AC voltage at high frequency is then rectified by the rectifier unit to charge the battery with constant DC voltage. The WPT coils are first simulated using Ansys Maxwell, and the values of leakage inductances and mutual inductances are used to simulate the complete charger in PSIM simulation platform. A scaled-down experimental prototype is developed in the laboratory to verify the proposed charger and tested to transfer 200 W power wirelessly over a distance of 12 cm. Finally, a 24 V, 30 Ah battery set is charged wirelessly using the proposed charger.

Data Availability

The data used to support the findings of this study are included within the article.

Conflicts of Interest

The authors declare that they have no conflicts of interest.

Acknowledgments

This work was supported by the Ministry of Electronics and Information Technology (MeitY), Government of India, under Project Sanction Order No. CDAC/EVS/PMU/0001.

References

[1] J. Cai and X. Zhao, "An on-board charger integrated power converter for EV switched reluctance motor drives," *IEEE Transactions on Industrial Electronics*, vol. 68, no. 5, pp. 3683–3692, 2021.

[2] S. Kim and F.-S. Kang, "Multifunctional onboard battery charger for plug-in electric vehicles," *IEEE Transactions on Industrial Electronics*, vol. 62, no. 6, pp. 3460–3472, 2015.

[3] D.-H. Kim, M.-J. Kim, and B.-K. Lee, "An integrated battery charger with high power density and efficiency for electric vehicles," *IEEE Transactions on Power Electronics*, vol. 32, no. 6, pp. 4553–4565, 2017.

[4] M. Tong, M. Cheng, S. Wang, and W. Hua, "An on-board two-stage integrated fast battery charger for EVs based on a five-phase hybrid-excitation flux-switching machine," *IEEE Transactions on Industrial Electronics*, vol. 68, no. 2, pp. 1780–1790, 2021.

[5] I. Subotic, N. Bodo, and E. Levi, "An EV drive-train with integrated fast charging capability," *IEEE Transactions on Power Electronics*, vol. 31, no. 2, pp. 1461–1471, 2016.

[6] S. Li and C. C. Mi, "Wireless power transfer for electric vehicle applications," *IEEE Journal of Emerging and Selected Topics in Power Electronics*, vol. 3, no. 1, pp. 4–17, 2015.

[7] Y. Li, J. Hu, X. Li et al., "Analysis, design, and experimental verification of a mixed high-order compensations-based WPT system with constant current outputs for driving multistring LEDs," *IEEE Transactions on Industrial Electronics*, vol. 67, no. 1, pp. 203–213, 2020.

[8] S. A. Q. Mohammed and J.-W. Jung, "A comprehensive state-of-the-art review of wired/wireless charging technologies for battery electric vehicles: classification/common topologies/future research issues," *IEEE Access*, vol. 9, pp. 19572–19585, 2021.

[9] F. Musavi and W. Eberle, "Overview of wireless power transfer technologies for electric vehicle battery charging," *IET Power Electronics*, vol. 7, no. 1, pp. 60–66, 2014.

[10] Z. Zhang, H. Pang, A. Georgiadis, and C. Cecati, "Wireless power transfer—an overview," *IEEE Transactions on Industrial Electronics*, vol. 66, no. 2, pp. 1044–1058, 2019.

[11] Z. Huang, S.-C. Wong, and C. K. Tse, "Design of a single-stage inductive-power-transfer converter for efficient EV battery charging," *IEEE Transactions on Vehicular Technology*, vol. 66, no. 7, pp. 5808–5821, 2017.

[12] T. Kan, T.-D. Nguyen, J. C. White, R. K. Malhan, and C. C. Mi, "A new integration method for an electric vehicle wireless charging system using LCC compensation topology: analysis and design," *IEEE Transactions on Power Electronics*, vol. 32, no. 2, pp. 1638–1650, 2017.

[13] M. Bojarski, E. Asa, K. Colak, and D. Czarkowski, "Analysis and control of multiphase inductively coupled resonant converter for wireless electric vehicle charger applications," *IEEE Transactions on Transportation Electrification*, vol. 3, no. 2, pp. 312–320, 2017.

[14] D. H. Tran, V. B. Vu, and W. Choi, "Design of a high-efficiency wireless power transfer system with intermediate coils for the on-board chargers of electric vehicles," *IEEE Transactions on Power Electronics*, vol. 33, no. 1, pp. 175–187, 2018.

[15] A. Ramezani, S. Farhangi, H. Iman-Eini, B. Farhangi, R. Rahimi, and G. R. Moradi, "Optimized LCC-Series compensated resonant network for stationary wireless EV chargers," *IEEE Transactions on Industrial Electronics*, vol. 66, no. 4, pp. 2756–2765, 2019.

[16] F. Liu, K. Chen, Z. Zhao, K. Li, and L. Yuan, "Transmitter-side control of both the CC and CV modes for the wireless EV charging system with the weak communication," *IEEE Journal of Emerging and Selected Topics in Power Electronics*, vol. 6, no. 2, pp. 955–965, June 2018.

[17] Y. Lin and Z. Zhao, "Topology and control strategy on transformerless wireless power station for future electric transportation systems," *International Transactions on Electrical Energy Systems*, vol. 31, no. 9, Article ID e130198, 2021.

[18] X. Wei, H. Sekiya, T. Nagashima, M. K. Kazimierczuk, and T. Suetsugu, "Steady-state analysis and design of class-D ZVS inverter at any duty ratio," *IEEE Transactions on Power Electronics*, vol. 31, no. 1, pp. 394–405, 2016.

[19] H. Sekiya, X. Wei, T. Nagashima, and M. K. Kazimierczuk, "Steady-state analysis and design of class-DE inverter at any duty ratio," *IEEE Transactions on Power Electronics*, vol. 30, no. 7, pp. 3685–3694, 2015.

[20] A. Ayachit, F. Corti, A. Reatti, and M. K. Kazimierczuk, "Zero-voltage switching operation of transformer class-E inverter at any coupling coefficient," *IEEE Transactions on Industrial Electronics*, vol. 66, no. 3, pp. 1809–1819, 2019.

[21] S. Aldhaher, D. C. Yates, and P. D. Mitcheson, "Modeling and analysis of class EF and class E/F inverters with series-tuned resonant networks," *IEEE Transactions on Power Electronics*, vol. 31, no. 5, pp. 3415–3430, 2016.

[22] S. Aldhaher, D. C. Yates, and P. D. Mitcheson, "Load-independent class E/EF inverters and rectifiers for MHz-switching applications," *IEEE Transactions on Power Electronics*, vol. 33, no. 10, pp. 8270–8287, 2018.